The role of Al^{3+}-based aqueous electrolytes in the charge storage mechanism of MnO_x cathodes

Véronique Balland, [†,*] *Mickaël Mateos,*[†] *Kenneth D. Harris,*[‡,§] *Benoît Limoges*[†,*]

[†] Université de Paris, Laboratoire d'Electrochimie Moléculaire, UMR CNRS 7591, F-75013 Paris, France.

[‡] National Research Council Canada, Nanotechnology Research Centre, Edmonton, Alberta, T6G 2M9, Canada

[§] Department of Mechanical Engineering, University of Alberta, Edmonton, Alberta, T6G 2V4, Canada

AUTHOR INFORMATION

Corresponding Author

* veronique.balland@u-paris.fr, * limoges@u-paris.fr

ABSTRACT. Rechargeable aqueous aluminium batteries are the subject of growing interest, but the charge storage mechanisms at manganese oxide-based cathodes remain poorly understood with as many mechanisms as studies. Here, we use an original *in situ* spectroelectrochemical methodology to unambiguously demonstrate that the reversible proton-coupled MnO_2-to-Mn^{2+} conversion is the main charge storage mechanism occurring at MnO_2 cathodes over a range of slightly acidic Al^{3+}-based aqueous electrolytes. In Zn/MnO_2 assemblies, this mechanism is associated with high gravimetric capacity and discharge potentials, up to 560 $mAh \cdot g^{-1}$ and 1.76 V respectively, attractive efficiencies (*CE* > 98.5 % and *EE* > 80%) and excellent cyclability (> 750 cycles at 10 $A \cdot g^{-1}$). Finally, we conducted a critical analysis of the data previously published on MnO_x cathodes in Al^{3+}-based aqueous electrolytes to conclude on a universal charge storage mechanism, *i.e.*, the reversible electrodissolution/electrodeposition of MnO_2.

Insertion of earth-abundant multivalent (MV) metal cations (*e.g.*, Mg^{2+}, Zn^{2+} and Al^{3+}) into host electrode materials is currently the subject of much attention due to the promising potential to go "beyond lithium". This is especially true with regard to the development of new insertion-based rechargeable aqueous batteries, which are currently under intensive study due to cost, safety and eco-sustainability considerations.[1,2] However, the real ability of multivalent cations to reversibly insert into redox-active materials, especially metal oxide-based hosts, is still uncertain.[3] Indeed, it has long been believed that the strong electrostatic interaction of MV cations with metal oxide lattices considerably hinders solid-state diffusivity,[4] leading to low electrochemical activity even in the presence of a strong thermodynamic driving force. Moreover, the high solvation energy of MV cations, especially in water, is an additional insertion barrier, adding to the difficulties of MV-ion insertion. Despite all of this, numerous recent works report the reversible insertion of MV cations into metal oxides in the presence of water, and under these conditions, they demonstrate electrochemical performances much better than in pure organic electrolytes.[5–7] However, a growing number of recent studies propose that the attractive performances observed with aqueous MV-ion batteries result from the reversible insertion of protons into the host electrode rather than MV cations. This has been evidenced in particular for VO_2,[8] V_2O_5,[9] $Na_3V_2(PO_4)_2F_3$,[10]and TiO_2[11] electrode materials cycled in either mild acidic Zn^{2+}- or Al^{3+}-based aqueous electrolytes. Moreover, in our previous work on TiO_2, we demonstrated that the source of protons in mild aqueous electrolytes was neither water nor H_3O^+, but the hexaaquo MV complexes (*e.g.*, $[Zn(H_2O)_6]^{2+}$, $[Al(H_2O)_6]^{3+}$) which spontaneously form in water to produce weak Brønsted acids.[11] More recently, we have also shown that the hexaaquo cations $[Zn(H_2O)_6]^{2+}$ and $[Mn(H_2O)_6]^{2+}$, commonly present in the aqueous electrolytes of Zn/MnO_2 batteries, can act as proton sources to trigger the electrodissolution of MnO_2 into Mn^{2+}.[12] These

studies underline the crucial, but little-known role played by the weak acidity of hydrated MV ions on the charge storage mechanisms at metal oxide electrodes. An illustration is provided by the trivalent Al^{3+} cation, which has recently been promoted for "rechargeable aqueous aluminium batteries", wherein an aluminium (or zinc) anode is paired with a MnO_x cathode in an Al^{3+}-based aqueous electrolyte.[13–18] A collective issue with these works, however, is the disparate variety of charge storage mechanisms and cathode compositions that are proposed. Indeed, some works suggest the reversible insertion of MV cations (Al^{3+} or Zn^{2+}) into either the pristine K_xMnO_2 phase[16] or an Al_xMnO_2 phase generated from a solid Mn_3O_4,[14] MnO[18] or MnO_2[17] precursor. Other reports assume a reversible conversion process, either solid-solid (*i.e.*, MnO_2-to-Mn_3O_4)[13] or solid-solute (*i.e.*, Al_xMnO_2-to-Mn^{2+}),[15] without clearly describing the role and source of protons.

In light of the numerous and contradictory mechanistic propositions, our objective with the present work is to decipher the exact role of Al^{3+} ions in the reversible charge storage mechanism of MnO_x cathodes immersed in Al^{3+}-based aqueous electrolytes. As we will see, our results unambiguously support a mechanism based on the reversible proton-coupled electrodissolution of solid MnO_x materials into soluble Mn^{2+} ions for a wide range of Al^{3+}-based electrolyte compositions, and they challenge the previously-reported charge storage mechanisms which are critically reviewed here.[13–18]

In the present work, MnO_x is quantitatively monitored during galvanostatic cycling by *in operando* UV-visible spectroelectrochemistry. This method was previously used to characterize amorphous MnO_2 within a 3D mesoporous transparent electrode (*i.e.,* a 1 µm-thick nanostructured ITO film deposited by glancing angle deposition (GLAD), over a flat ITO-coated glass substrate – see Scheme 1).[12,19] Here, we prepare similar MnO_2-GLAD-ITO electrodes (see

Experimental Section for details and Fig. S1 and S2)[19] by systematically applying 100 $mC \cdot cm^{-2}$ to the nanocolumnar GLAD-ITO electrodes, which is equivalent to 48 ± 1 $\mu g \cdot cm^{-2}$ MnO_2.[19] XRD and XPS analysis of the electrodeposited material show that MnO_2 is amorphous and characterized by an average Mn oxidation state of 3.86.[19] Accordingly, the maximal theoretical gravimetric capacity of these MnO_2-GLAD-ITO electrodes is 574 $mA \cdot h \cdot g^{-1}$. Their electrochemical reactivity was examined with/without Al^{3+} in a three-electrode cell configuration in different aqueous electrolytes adjusted to pH 2.0 (see Table S1 for chemical compositions). The spectroelectrochemical data associated with the first galvanostatic discharges are given in Fig. 1A and 1B.

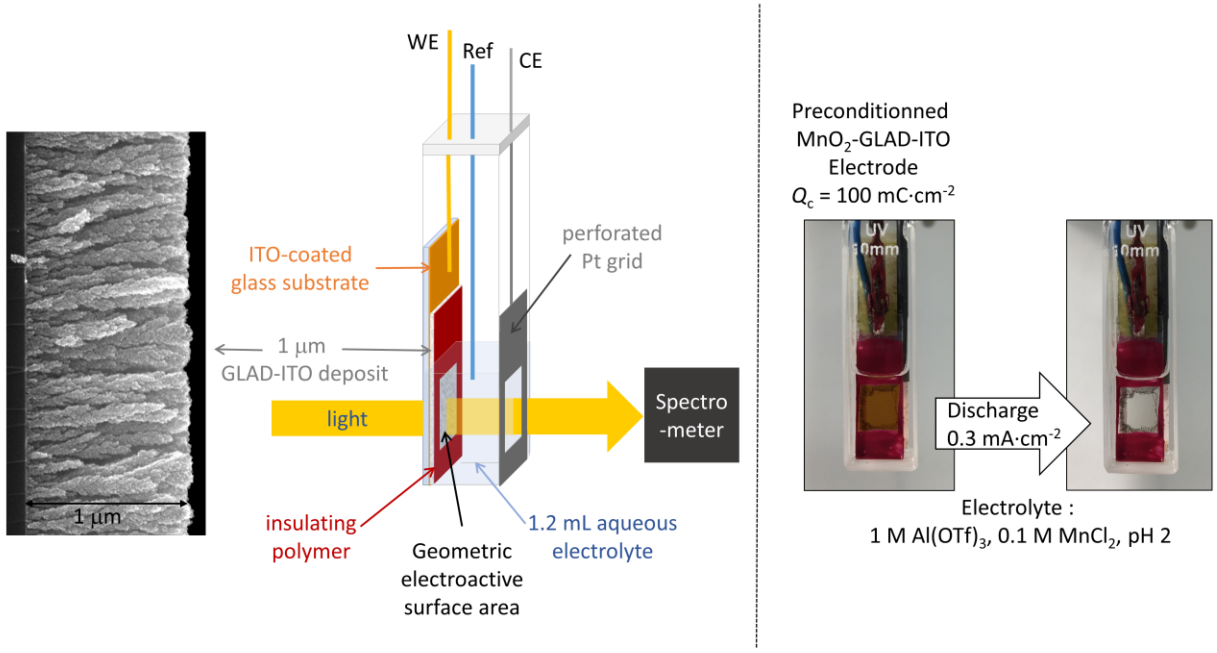

Scheme 1. Left: schematic of the *in operando* spectroelectrochemical setup used to monitor a MnO_2-loaded GLAD-ITO electrode (made of a 1-µm thick transparent nanostructured film of GLAD-ITO). Right: photographs of the spectroelectrochemical cell taken at the beginning and end of a galvanostatic discharge experiment performed at a GLAD-ITO electrode loaded *ex situ*.

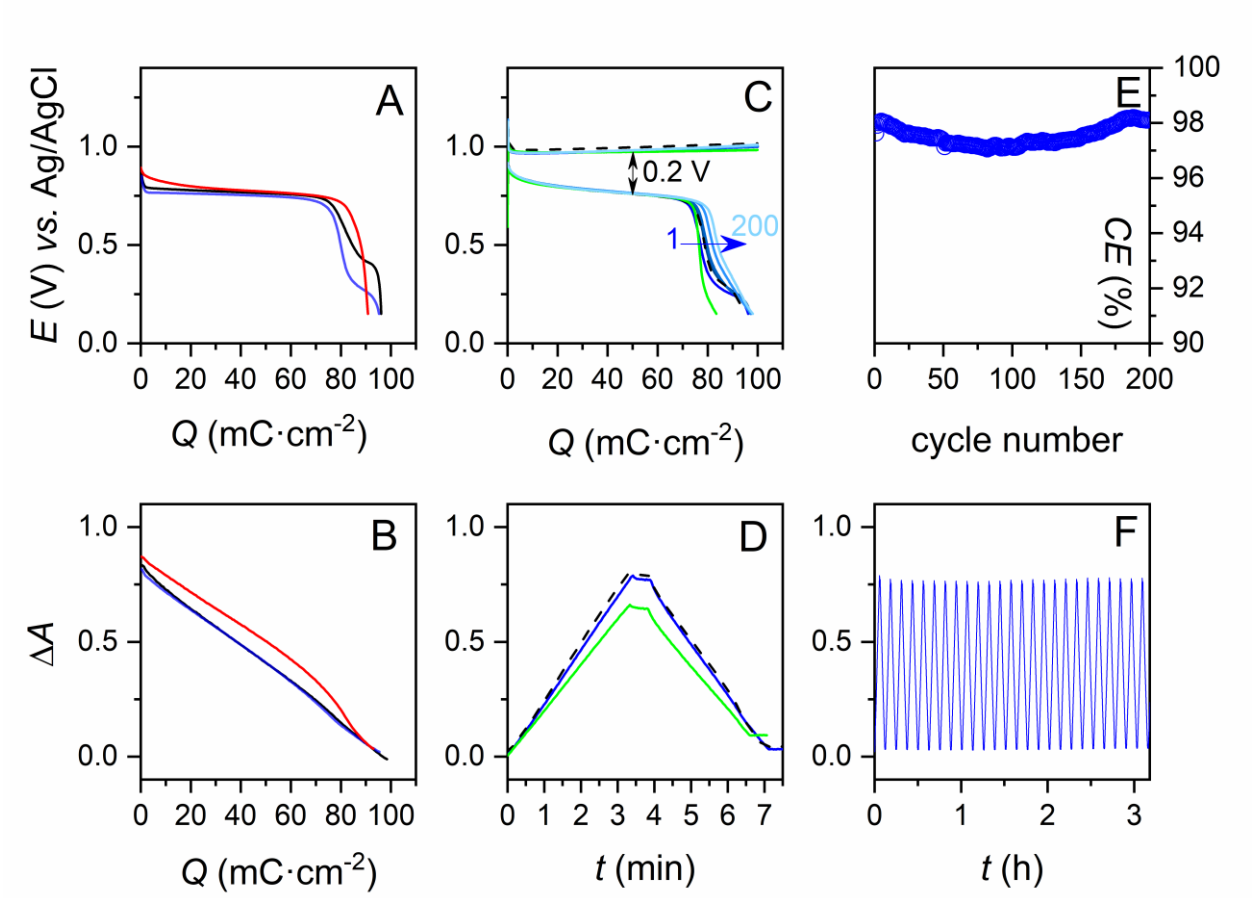

Figure 1. *In operando* spectroelectrochemical characterization of MnO_2-GLAD-ITO electrodes in different aqueous electrolytes (adjusted to pH 2). (A) Galvanostatic curves (rate: 0.3 $mA \cdot cm^{-2}$) and (B) absorbance variations concomitantly recorded during the first discharge of a MnO_2-GLAD-ITO electrode (loaded *ex situ* with a deposited charge of 100 $mC \cdot cm^2$) immersed in the following electrolytes: (red) 1 M acetic acid + 0.1 M $MnCl_2$ + 2 M KCl, (blue) 1 M $Al(OTf)_3$ + 0.1 M $MnCl_2$, and (black) 1 M $AlCl_3$ + 0.1 M $MnCl_2$. (C) Galvanostatic charge/discharge curves (rate: 0.3 $mA \cdot cm^{-2}$) and (D, F) absorbance variations concomitantly recorded at a GLAD-ITO electrode cycled in an aqueous electrolyte containing: (blue) 1 M $Al(OTf)_3$ + 0.1 M $MnCl_2$, (dashed black) 1 M $AlCl_3$ + 0.1 M $MnCl_2$, and (green) 1.4 M $Al(OTf)_3$ + 7.1 mg/L MnO (see text for details). (E) Coulombic efficiencies (*CE*) recovered from the continuous galvanostatic experiment reported in (C) and (F).

In a 1 M acetic acid (pH 2.0) electrolyte, the galvanostatic discharge curve is characterized by a well-defined single plateau (red line in Fig. 1A), leading to an areal discharge capacity (C_d) of 92 mC·cm^{-2} (Table S1) close to the *ex situ* deposited charge of 100 mC·cm^{-2} (thus a Coulombic efficiency of CE = 92%). Concomitantly, the absorbance of the electrode decreases almost linearly to near zero (red line in Fig. 1B). These observations are in line with those we have recently reported[19] in a 1 M acetate buffer of pH 5 and support the following proton-coupled electron transfer reaction, in which acetic acid is involved as a proton donor:

$$Mn^{IV}O_2 + 4\ CH_3COOH + 4\ H_2O + 2\ e^- \rightarrow [Mn^{II}(H_2O)_6]^{2+} + 4\ CH_3COO^- \qquad (1)$$

The near complete electrodissolution of MnO_2 is further confirmed by the low m_{MnO_2} value obtained for the discharged electrode (Table S1), indicating that only ~4% of the initially electrodeposited Mn remains on the electrode. As a result, the discharge gravimetric capacity is 530 mA·h·g^{-1}, close to the theoretical value.

The half-discharge potential (E_d) of 0.74 V (*vs.* Ag/AgCl) is significantly higher than that previously reported in a 1 M acetate buffer of pH 5 (E_d = 0.50 V).[12,19] This can be easily explained from the lower electrolyte pH here and the Nernst equation derived from reaction 1 (see eq. S1).[12] However, to accurately interpret the E_d value, it is important to consider that the local pH at the MnO_2/electrolyte interface can differ from the bulk and is indeed expected to rise significantly during the MnO_2 electrodissolution (according to the stoichiometry of reaction 1 and the unbuffered electrolyte). Using eq. S1 and assuming that the process remains near thermodynamic equilibrium, the E_d value of 0.74 V translates into a local pH of ~3, thus slightly higher than the bulk pH 2. This agrees with a local conversion of acetic acid into acetate, which,

as a function of their respective local activities and pK_a (4.74), determine the local pH (see SI for details).

It is worth noting that at pH 2, the concentration of free protons (*i.e.*, H_3O^+) remains too low (~10^{-2} M) to trigger the reductive electrodissolution of MnO_2 in an inert KCl electrolyte (see Fig. S4 and associated text), whereas at pH 1, the H_3O^+ concentration becomes sufficient (~0.1 M) to ensure full proton-coupled electrodissolution of MnO_2 (see Fig. S4 and Table S1). This behaviour is consistent with recent reports for rechargeable aqueous Zn/MnO_2 batteries operating in strongly acidic electrolytes.[20,21] As a consequence for further study, we deliberately avoided the overly concentrated Al^{3+}-based electrolytes (common in the literature) as they leads to very low pHs (Table S2) and so prevailing participation of H_3O^+ in the discharge process. In Fig. 1A and 1B, the data recorded during the first galvanostatic discharge of MnO_2-GLAD-ITO electrodes in 1 M $Al(OTf)_3$ and 1 M $AlCl_3$ aqueous electrolytes (pH 2) are also overlaid. The shapes and positions of the discharge and absorption curves are almost identical to those recorded in the 1 M acetic acid, the only difference being the appearance of a poorly-defined secondary discharge plateau, located at a lower potential. We do not believe these secondary plateaus are linked to aluminium ions in the electrolyte since they were previously observed in an Al^{3+}-free acidic electrolyte.[21] Alternatively, we suspect it could be related to the denucleation process, which may be more difficult at the end of the discharge. For either Al^{3+}-based electrolyte, a full recovery of the electrode transparency was observed (see pictures in Scheme 1), demonstrating full electrodissolution of MnO_2. This was also corroborated by both the high CE > 96% and small m_{MnO_2} values after discharge (see Table S1). Accordingly, an exploitable gravimetric capacity as high as 550 mA·h·g^{-1} could be achieved, almost identical to the value in 1 M acetic acid. These observations lead to the irrefutable conclusion that we are dealing with a

two-electron MnO_2-to-Mn^{2+} conversion mechanism, involving protons (or proton donors) as the charge carriers.

Another interesting feature of the discharge curves in Fig. 1A is their almost identical half-discharge potential values (Table S1), which indicates similar local pHs at the MnO_2 surfaces regardless the nature of the electrolyte. This implies that the proton donors involved in the conversion reactions are weak Brønsted acids of similar strength (*i.e.,* close pK_a). Given that the hexaaquo complex $[Al(H_2O)_6]^{3+}$ has a weak Brønsted acidity (pK_a = 4.9)[22] comparable to that of acetic acid (pK_a = 4.76), we propose by analogy to reaction 1, the following proton-coupled MnO_2-reductive electrodissolution reaction 2 in the Al^{3+}-based aqueous electrolytes (in which $[Al(H_2O)_6]^{3+}$ plays the role of a proton donor):

$$Mn^{IV}O_2 + 4\ [Al(H_2O)_6]^{3+} + 4\ H_2O + 2\ e^- \rightarrow [Mn^{II}(H_2O)_6]^{2+} + 4\ [Al(H_2O)_5(OH)]^{2+} \qquad (2)$$

Once completely discharged, the electrodes were subjected to a galvanostatic charge of 100 $mC \cdot cm^{-2}$ at a rate of 0.5 $mA \cdot cm^{-2}$. The data recorded in 1 M $Al(OTf)_3$ containing 0.1 M $MnCl_2$ are reported in Fig. 1C to 1F (blue curves). During the charge, the potential rapidly stabilizes at 0.98 V, while the absorbance of the electrode increases linearly (Fig. 1D), confirming a steady electrodeposition of MnO_2 to an amount close to that achieved for the electrodes loaded *ex situ*. Interestingly, similar results were obtained with a fresh GLAD-ITO electrode charged *in situ* in the same electrolyte (see black dashed lines in Fig. 1C and 1D), confirming that the MnO_2 electrodeposition remains effective under these conditions.

Owing to the conversion mechanism, the electrodeposition of MnO_2 requires the presence of soluble Mn^{2+} ions in the electrolyte. This is commonly achieved by adding a highly soluble inorganic Mn^{2+} salt to the electrolyte. However, as shown below, it can also be achieved from a

solid precursor such as MnO, calling into question the recent work of Yan *et al.* on the reversible insertion of Al^{3+} in MnO.[18] Indeed, in agreement with the Pourbaix diagram of manganese, it has been shown that MnO is prone to dissolve in slightly acidic media.[23] To demonstrate that MnO can effectively dissolve in an Al^{3+}-based electrolyte, we added MnO to a 2 m $Al(OTf)_3$ electrolyte (*i.e.,* the same electrolyte used in ref. 18, see Experimental Section). The resulting electrolyte was then used to cycle a fresh GLAD-ITO electrode. The results in Fig. 1C and 1D (green lines) show the successful electrodeposition/electrodissolution of MnO_2 under these conditions, thereby confirming the spontaneous dissolution of MnO to Mn^{2+} in the Al^{3+}-based electrolyte. XRF analysis of the charged electrode indicates an electrodeposited m_{MnO_2} value of 44 $\mu g \cdot cm^{-2}$, comparable to that obtained with electrodes loaded *ex situ*. We were unable to discern aluminium in the XRF spectrum of the charged electrode, suggesting the absence of an Al_xMnO_2 phase in contrast to what was previously reported.[18]

The continuous galvanostatic cycling of the GLAD-ITO electrode in the 1 M $Al(OTf)_3$ electrolyte containing 0.1 M $MnCl_2$ (see Fig. 1E and data in Table S2) demonstrates a remarkably stable and high *CE* (~97.5 % over 200 cycles), which correlates well with the stable periodic electrode absorbance variations monitored during the first 3 hours of cycling (Fig. 1F). In addition, apart from the secondary discharge plateaus that tend to progressively weaken, the galvanostatic charge/discharge curves almost overlap during cycling. These results are consistent with a complete and highly reversible electrodeposition-electrodissolution conversion process, without significant accumulation of MnO_2 or any other MnO_x material. It is worth noting that aluminium was below the limit of quantification in all the charged and discharged electrodes investigated by XRF. This confirms that the Al_xMnO_2 phase suggested in several works[14,15,17,18]

is not formed and also that the electrolyte is properly removed by thoroughly rinsing the electrode with water prior to *ex situ* analysis.

We next investigated the cyclability of the MnO_2-GLAD-ITO electrode in a Zn/MnO_2 cell configuration (two-electrode cell, see Experimental Section for details) with the electrolytes listed in Table S3 (containing Zn^{2+} to allow for the reversible Zn^{2+}-to-Zn conversion reaction at the anode). First, we verified that addition of 0.25 M $ZnCl_2$ to the 1 M $AlCl_3$ + 0.1 M $MnCl_2$ electrolyte does not significantly affect the reversibility and efficiency of the MnO_2-to-Mn^{2+} conversion reaction. This was confirmed from the high *CE* of the galvanostatic cycles (Fig. 2A, 2C and Table S3) and the stable absorbance change recorded during cycling (Fig. 2B). Also in this electrolyte, the Zn/MnO_2 cell delivers an excellent and stable discharge gravimetric capacity of ~560 $mA \cdot h \cdot g_{MnO2}^{-1}$ over 100 cycles (one of the best gravimetric capacities reported for a Zn/MnO_2 cell). The cell also displays a remarkably high discharge voltage (~1.7 V) as well as an excellent energetic efficiency (*EE* > 80% at 10 $A \cdot g^{-1}$).

The data presented in Fig. 2 and Table S3 show that the chemical composition of the Al^{3+}-based aqueous electrolytes has little effect on the shape and position of the galvanostatic charge/discharge curves. That all Zn/MnO_2 assemblies have such similar electrochemical features indicates they share a common charge storage mechanism that we attribute to the following dual reversible conversion process:

$$MnO_{2(s)} + 4\ [Al(H_2O)_6]^{3+} + Zn \leftrightarrows Mn^{2+}_{(aq)} + 4\ [Al(H_2O)_5(OH)]^{2+} + 2\ H_2O + Zn^{2+}_{(aq)} \qquad (3)$$

This mechanism is further supported by the excellent gravimetric capacity we have systematically retrieved (*i.e.* > 550 $mA \cdot h \cdot g_{MnO2}^{-1}$), which interestingly is comparable to the value

recently achieved in a strongly acidic electrolyte where the reversible proton-coupled conversion of MnO_2 into Mn^{2+} was fully established (see Table 1).[21]

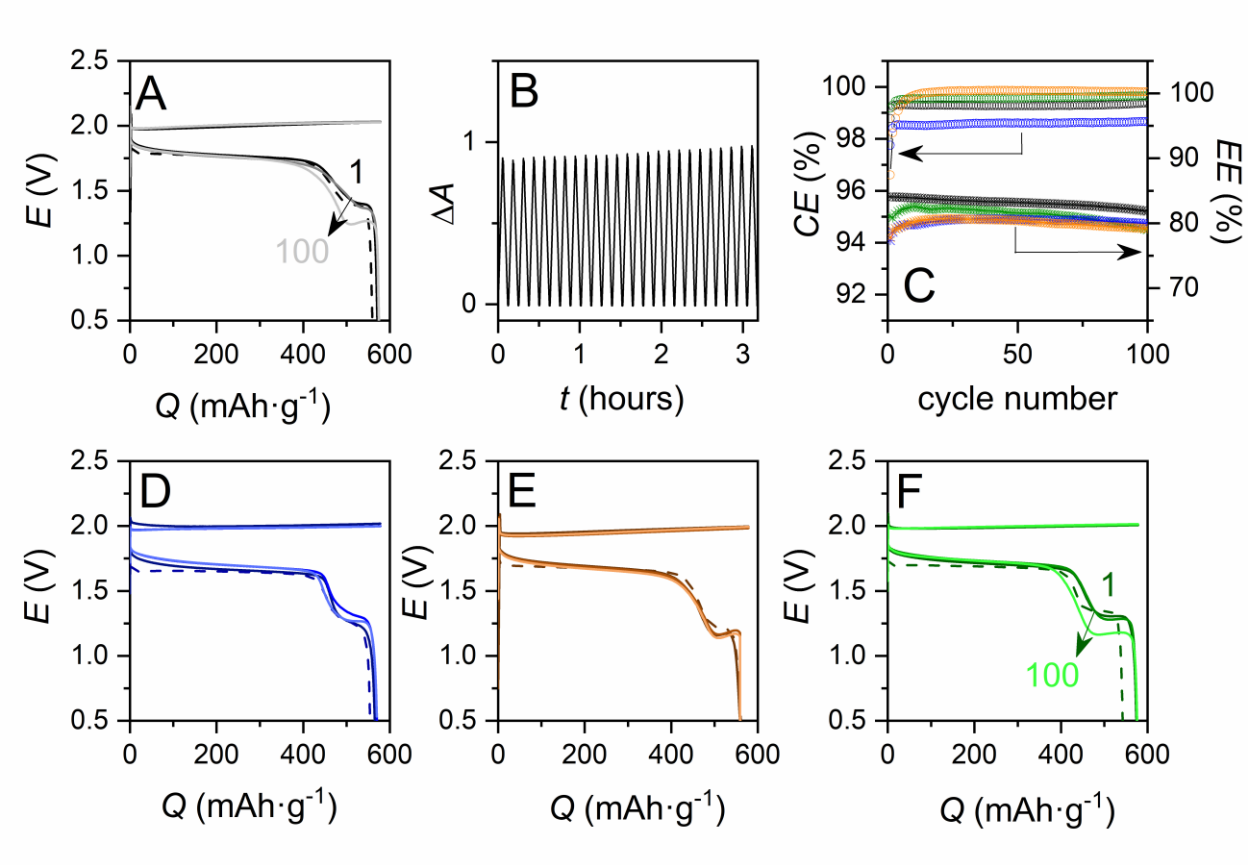

Figure 2. Galvanostatic cycles performed at a Zn foil/MnO_2-GLAD-ITO cell assembly (loaded *ex situ* with 48 $\mu g_{MnO2} \cdot cm^{-2}$) in the presence of the following Al^{3+}-based aqueous electrolytes: (A, B) 1 M $AlCl_3$ + 0.25 M $ZnCl_2$ + 0.1 M $MnCl_2$ (pH 1.90), (D) 1 M $Al(OTf)_3$ + 0.1 M $ZnCl_2$ + 0.1 M $MnCl_2$ (pH 1.77), (E) 1 m $Al(OTf)_3$ + 1 m $Zn(OTf)_3$ + 0.1 m $MnSO_4$ (pH 1.75), and (F) 1.25 M $Al(OTf)_3$ + 0.1 M $ZnCl_2$ + 0.1 M $MnCl_2$ (pH 1.5). The dashed black lines correspond to the 1st galvanostatic discharges (recorded at 0.3 $mA \cdot cm^{-2}$), while the solid lines are galvanostatic charge/discharge cycles (100 cycles at 0.5 $mA \cdot cm^{-2}$ with the 1st, 50th and 100th cycles shown). (C) Cycling performances of the Zn/MnO_2 cell assemblies mentioned in A to F (same color code).

Table 1. Chemical composition and pH of the aqueous electrolytes used in Zn/MnO_2 or Al/MnO_2 assemblies and the main features of the galvanostatic cycling, *i.e.* rate, half-charge (E_c) and half-discharge (E_d) potentials, maximal discharge capacity, and Coulombic efficiency (*CE*).

electrolyte composition	pH	Anode	Rate ($A \cdot g^{-1}$)	E_d (V)	E_c (V)	*CE*	Maximal discharge capacity ($mA \cdot h \cdot g_{MnO2}^{-1}$)	cathode mechanism	*Ref*
1 M $Al(OTf)_3$, 0.1 M $ZnCl_2$, 0.1 M $MnCl_2$	1.77	Zn	10	1.65	1.99	98.8 % over 250 cycles at 10 $A \cdot g^{-1}$	560	$MnO_2 \leftrightarrow Mn^{2+}$	This work
1 m $Al(OTf)_3$, 1 m $Zn(OTf)_3$, 0.1 m $MnSO_4$	1.75	Zn	10	1.65	1.95	99.7 % over 600 cycles at 10 $A \cdot g^{-1}$	570	$MnO_2 \leftrightarrow Mn^{2+}$	This work
1 M $ZnSO_4$, 1 M $MnSO_4$, 0.1 M H_2SO_4	1	Zn	0.58	1.95	amperometry at 2.2 V	92 % after 1800 cycles at 8.6 $A \cdot g^{-1}$	570	$MnO_2 \leftrightarrow Mn^{2+}$	21
1 M $Al(OTf)_3$, 1 M $Zn(OTf)_3$, 0.1 M $MnSO_4$	*ns*	Zn	0.1	~1.55	1.8	~100% over 1000 cycles at 1 C	264	Reversible co-insertion of Zn^{2+} and H^+in Al_xMnO_2	17
2 M $Al(OTf)_3$	*ns*	Zn/Al alloy	0.1	1.6	1.8	~75% after 80 cycles at 0.1 $A \cdot g^{-1}$	460	$Al_xMnO_2 \leftrightarrow$ MnO with reversible uptake of Al^{3+}	18
2 m $Al(OTf)_3$, 0.1 m $Mn(OTf)_2$	*ns*	T-Al [a]	0.1	1.3	~1.6	~50% after 100 cycles at 0.2 $A \cdot g^{-1}$	310	$MnO_2 \leftrightarrow Mn_3O_4$	13
2 M $Al(OTf)_3$, 0.5 M $MnSO_4$	*ns*	T-Al [a]	0.1	1.3→1.15	1.6	~55% after 70 cycles at 0.1 $A \cdot g^{-1}$	554	$Al_xMn_{(1-x)}O_2 \leftrightarrow Mn^{2+}$	15
5 M $Al(OTf)_3$	< -0.5	Al	0.03	1.2 & 0.8	1.65	~60% after 65 cycles	467	Reversible Al^{3+} insertion in $Al_{x=0.1}MnO_2$	14

ns: not specified

[a] Aluminium anode pre-treated in an ionic liquid

We also tested the so-called bi-cation electrolyte (1 m $Al(OTf)_3$ + 1 m $Zn(OTf)_2$ + 0.1 m $MnSO_4$) used in ref. 17. Again, no significant change was observed in the charge/discharge curves (Figure 2E), which confirms that the charge storage mechanism described above remains at work. This is in sharp contrast with the previously proposed mechanism based on the reversible co-insertion of H^+ and Zn^{2+} in an Al_xMnO_2 phase generated *in situ* (see further comment on pH considerations in the SI).[17] In such bi-cation electrolytes, the cyclability was actually improved with 100% capacity retention over 600 cycles (see Table 1), demonstrating the high reversibility of the dual conversion process.

Overall, the present results shed new light on the aqueous aluminium batteries pairing a manganese oxide cathode with an aluminium or zinc anode,[13–18] for which the electrochemical features are gathered in Table 1. It is striking that cells based on identical anodes and electrolytes with similar pHs share similar electrochemical features (notably charge/discharge potentials), a behaviour suggesting thermodynamically equivalent electrochemical processes. On the basis of the present results, it is quite clear that MnO_x to Mn^{2+} conversion is a robust and invariable process independent of the nature of the cathode and/or Al^{3+}-based electrolyte. In view of this behavior, the diversity of mechanisms proposed in the literature (summarized in Table 1) raises questions, as it is very possible that a unified mechanism drives all the Al/MnO_x or Zn/MnO_x aqueous batteries gathered in Table 1.

One may however argue that complementary material characterization techniques are required to better probe our active material and to support the proposed unified charge storage mechanism. However, the characterization techniques based on *ex situ* or *in operando* spectroscopic analysis of the charged/discharged materials, such as XRD, XPS and elemental mapping analysis, are inconveniently blind to the dissolution processes and may mislead the

interpretation of the charge storage mechanism. This is especially true for the reduced state Mn^{2+}, which once solubilised in the electrolyte, is no longer detectable by such techniques. Another difficulty is the amorphous state of the back electrogenerated MnO_x material, which unfortunately cannot be characterized by XRD. Despite this, several studies speculate on the *in situ* formation of a layered Al_xMnO_2 phase based on the detection of Al in the XPS spectra and energy dispersive spectroscopy mappings.[14,15,17,18] However, this is insufficient to irrefutably demonstrate the formation of an Al_xMnO_2 phase,[14,15,17,18] and to assert that Al^{3+} can reversibly insert into this phase.[14,18]

Another important aspect that is often improperly considered is that the cyclability of the Zn/MnO_2 batteries improves when sufficient Mn^{2+} (0.1 to 0.5 M) is added into the Al^{3+}-based electrolytes.[13,15,17] Rather than inhibiting the dissolution of Mn^{2+}, we and other groups demonstrated that the role of pre-added Mn^{2+} in the aqueous electrolytes is to act as a reservoir for MnO_2 electrodeposition during charging.[12,24,25] This is the principle of a conversion battery, where the capacity of the electrolyte has to be taken into account for the energy density calculation.

Some publications report on lower oxidation state manganese oxide cathode materials (*i.e.*, spinel Mn_3O_4 and MnO) capable of cycling in highly concentrated $Al(OTf)_3$ aqueous electrolytes free of Mn^{2+} ions.[14,18] The problem with such oxides is that they tend to spontaneously dissolve in acidic electrolytes,[23, 25] as we have shown here with MnO. Because of the rather high concentration of $Al(OTf)_3$ used in these studies (>2 M at pH < 0, see Table S2), Mn^{2+} is expected to be generated *in situ* from the spontaneous dissolution of the Mn_3O_4- or MnO-based cathode. After a certain time, a significant amount of Mn^{2+} is thus present in these electrolytes, fulfilling the requirements for a reversible MnO_2-to-Mn^{2+} conversion.

Finally, some authors suggest the reversible insertion of multivalent cations (Al^{3+} or Zn^{2+}) in an *in situ* activated layered phase of Al_xMnO_2.[14,17] The present study clearly demonstrates that neither Al^{3+} nor Zn^{2+} can reversibly insert in the active MnO_x phase, which is totally dismantled through the proton-coupled electrodissolution process.

To conclude, the present study unambiguously demonstrates that the reversible proton-coupled MnO_2-to-Mn^{2+} conversion is the main charge storage mechanism of MnO_x-based cathodes when cycled in Al^{3+}-based aqueous electrolytes. By avoiding excessively high concentrations of Al^{3+} ions associated with strongly acidic conditions, we highlighted the essential role of the $[Al(H_2O)_6]^{3+}$ complex as a proton donor, allowing exploitation of the 2 electron charge storage capacity of MnO_2 with high cyclability and efficiency. The nature of the counter ions has little effect over the charge storage, making MnO_2-to-Mn^{2+} conversion a robust mechanism that is was likely unknowingly involved in previous studies.

Supporting Information. Experimental section, Supplementary Figures S1 to S6, and Tables S1 to S3and additional comments are provided in the Supporting Information file.

Corresponding Authors:

*E-mail: veronique.balland@u-paris.fr.

*E-mail: limoges@u-paris.fr

ORCID:

Véronique Balland: 0000-0001-9534-9659

Benoît Limoges: 0000-0002-2466-1896

ACKNOWLEDGMENT

The authors thank Ivonne Cocca and Sophie Nowak (Université de Paris) for X-Ray fluorescence measurements. We also gratefully acknowledge financial support from the French National Agency (ANR AqReBat project).

REFERENCES

(1) Shin, J.; Choi, J. W. Opportunities and Reality of Aqueous Rechargeable Batteries. *Adv. Energy Mater.* **2020**, 2001386. https://doi.org/10.1002/aenm.202001386.

(2) Chao, D.; Zhou, W.; Xie, F.; Ye, C.; Li, H.; Jaroniec, M.; Qiao, S. Roadmap for Advanced Aqueous Batteries : From Design of Materials to Applications. *Sci. Adv.* **2020**, *6*, eaba4098.

(3) Park, M. J.; Asl, H. Y.; Manthiram, A. Multivalent-Ion versus Proton Insertion into Battery Electrodes. *ACS Energy Lett.* **2020**, *5*, 2367–2375. https://doi.org/10.1021/acsenergylett.0c01021.

(4) Rong, Z.; Malik, R.; Canepa, P.; Sai Gautam, G.; Liu, M.; Jain, A.; Persson, K.; Ceder, G. Materials Design Rules for Multivalent Ion Mobility in Intercalation Structures. *Chem. Mater.* **2015**, *27* (17), 6016–6021. https://doi.org/10.1021/acs.chemmater.5b02342.

(5) Mathew, V.; Sambandam, B.; Kim, S.; Kim, S.; Park, S.; Lee, S.; Alfaruqi, M. H.; Soundharrajan, V.; Islam, S.; Putro, D. Y.; Hwang, J.; Sun, Y.; Kim, J. Manganese and Vanadium Oxide Cathodes for Aqueous Rechargeable Zinc-Ion Batteries: A Focused View on Performance, Mechanism, and Developments. *ACS Energy Lett.* **2020**, *5*, 2376–2400. https://doi.org/10.1021/acsenergylett.0c00740.

(6) Manalastas, W.; Kumar, S.; Verma, V.; Zhang, L.; Yuan, D. Water in Rechargeable Multivalent-Ion Batteries : An Electrochemical Pandora's Box. *ChemSusChem* **2019**, *12*, 379–396. https://doi.org/10.1002/cssc.201801523.

(7) Liu, T.; Cheng, X.; Yu, H.; Zhu, H.; Peng, N.; Zheng, R. An Overview and Future Perspectives of Aqueous Rechargeable Polyvalent Ion Batteries. *Energy Storage Mater.* **2019**, *18* (June 2018), 68–91. https://doi.org/10.1016/j.ensm.2018.09.027.

(8) Li, Z.; Ganapathy, S.; Xu, Y.; Zhou, Z.; Sarilar, M.; Wagemaker, M. Mechanistic Insight into the Electrochemical Performance of Zn/VO_2 Batteries with an Aqueous $ZnSO_4$ Electrolyte. *Adv. Energy Mater.* **2019**, *1900237*, 1–10. https://doi.org/10.1002/aenm.201900237.

(9) Zhao, Q.; Liu, L.; Yin, J.; Zheng, J.; Zhang, D.; Chen, J.; Archer, L. Proton Intercalation/de-Intercalation Dynamics in Vanadium Oxides for Aqueous Aluminum Electrochemical Cells. *Angew. Chemie Int. Ed.* **2020**, *59*, 1–6. https://doi.org/10.1002/anie.201912634.

(10) Park, M. J.; Manthiram, A. Unveiling the Charge Storage Mechanism in Nonaqueous and Aqueous Zn/$Na_3V_2(PO_4)_2F_3$ Batteries. *ACS Appl. Energy Mater.* **2020**, *3*, 5015–5023. https://doi.org/10.1021/acsaem.0c00505.

(11) Kim, Y.-S.; Harris, K. D.; Limoges, B.; Balland, V. On the Unsuspected Role of Multivalent Metal Ions on the Charge Storage of a Metal Oxide Electrode in Mild Aqueous Electrolytes. *Chem. Sci.* **2019**, *10* (38), 8752–8763. https://doi.org/10.1039/c9sc02397f.

(12) Mateos, M.; Makivic, N.; Kim, Y.-S.; Limoges, B.; Balland, V. Accessing the Two-Electron Charge Storage Capacity of MnO_2 in Mild Aqueous Electrolytes. *Adv. Energy Mater.* **2020**, 2000332. https://doi.org/10.1002/aenm.202000332.

(13) Zhao, Q.; Zachman, M. J.; Sadat, W. I. Al; Zheng, J.; Kourkoutis, L. F.; Archer, L. Solid Electrolyte Interphases for High-Energy Aqueous Aluminum Electrochemical Cells. *Sci. Adv.* **2018**, *4* (November), eaau8131.

(14) Wu, C.; Gu, S.; Zhang, Q.; Bai, Y.; Li, M.; Yuan, Y.; Wang, H.; Liu, X.; Yuan, Y.; Zhu, N.; Wu, F.; Li, H.; Gu, L.; Lu, J. Electrochemically Activated Spinel Manganese Oxide

for Rechargeable Aqueous Aluminum Battery. *Nat. Commun.* **2019**, *10* (1), 73. https://doi.org/10.1038/s41467-018-07980-7.

(15) He, S.; Wang, J.; Zhang, X.; Chen, J.; Wang, Z.; Yang, T.; Liu, Z.; Liang, Y.; Wang, B.; Liu, S.; Zhang, L.; Huang, J.; Huang, J.; Dell, L. A. O.; Yu, H. A High-Energy Aqueous Aluminum-Manganese Battery. *Adv. Funct. Mater.* **2019**, 1905228. https://doi.org/10.1002/adfm.201905228.

(16) Joseph, J.; Nerkar, J.; Tang, C.; Du, A.; O'Mullane, A. P.; Ostrikov, K. Reversible Intercalation of Multivalent Al_{3+} Ions into Potassium-Rich Cryptomelane Nanowires for Aqueous Rechargeable Al-Ion Batteries. *ChemSusChem* **2019**, *12* (16), 3753–3760. https://doi.org/10.1002/cssc.201901182.

(17) Li, N.; Li, G.; Li, C.; Yang, H.; Qin, G.; Sun, X.; Li, F.; Cheng, H. Bi-Cation Electrolyte for a 1.7 V Aqueous Zn Ion Battery. *ACS Appl. Mater. Interfaces* **2020**, *12*, 13790–13796. https://doi.org/10.1021/acsami.9b20531.

(18) Yan, C.; Lv, C.; Wang, L.; Cui, W.; Zhang, L.; Dinh, K. N.; Tan, H.; Wu, C.; Wu, T.; Ren, Y.; Chen, J.; Liu, Z.; Srinivasan, M.; Rui, X. Architecting a Stable High-Energy Aqueous Al-Ion Battery. *J. Am. Chem. Soc.* **2020**, *142*, 15295615304. https://doi.org/10.1021/jacs.0c05054.

(19) Mateos, M.; Harris, K. D.; Limoges, B.; Balland, V. Nanostructured Electrode Enabling Fast and Fully Reversible MnO_2-to-Mn^{2+} Conversion in Mild Buffered Aqueous Electrolytes. *ACS* **2020**, *3*, 7610–7618. https://doi.org/10.1021/acsaem.0c01039.

(20) Chen, W.; Li, G.; Pei, A.; Li, Y.; Liao, L.; Wang, H.; Wan, J.; Liang, Z.; Chen, G.; Zhang, H.; Wang, J.; Cui, Y. A Manganese-Hydrogen Battery with Potential for Grid-Scale Energy Storage. *Nat. Energy* **2018**, *3* (5), 428–435. https://doi.org/10.1038/s41560-018-

0147-7.

(21) Chao, D.; Zhou, W.; Ye, C.; Zhang, Q.; Chen, Y.; Gu, L.; Davey, K.; Qiao, S. Z. An Electrolytic Zn–MnO_2 Battery for High-Voltage and Scalable Energy Storage. *Angew. Chemie - Int. Ed.* **2019**, 7823–7828. https://doi.org/10.1002/anie.201904174.

(22) *CRC Hanbook of Chemistry and Physics*, Internet V.; Lide, D. R., Ed.; CRC Press, Bocan Raton, FL, 2005.

(23) Jones, C. F.; St, R.; Smart, C.; Turner, P. S. Dissolution Kinetics of Manganese Oxides. *J. Chem. Soc. Faraday Trans.* **1990**, *86* (6), 947–953.

(24) Yang, J.; Cao, J.; Peng, Y.; Yang, W.; Barg, S.; Liu, Z.; Kinloch, I. A.; Bisset, M. A.; Dryfe, R. A. W. Unravelling the Mechanism of Rechargeable Aqueous Zn–MnO_2 Batteries : Implementation of Charging Process by Electrodeposition of MnO_2. *ChemSusChem* **2020**, *13*, 4103–4110. https://doi.org/10.1002/cssc.202001216.

(25) Wu, D.; Housel, L. M.; Kim, J.; Sadique, N.; Quilty, C. D.; Wu, L.; Tappero, R.; Nicholas, S. L.; Ehrlich, S.; Zhu, Y.; Marschilok, A. C.; Takeuchi, E. S.; Bock, D. C.; Takeuchi, K. J. Environmental Science Quantitative Temporally and Spatially Resolved X-Ray Fluorescence Microprobe Characterization of the Manganese Dissolution-Deposition Mechanism in Aqueous Zn/α-MnO_2 Batteries. *Energy Environ. Sci.* **2020**, *13*, 4322–4333. https://doi.org/10.1039/D0EE02168G.

(26) Artamonova, I. V.; Gorichev, I. G.; Godunov, E. B. Kinetics of Manganese Oxides Dissolution in Sulphuric Acid Solutions Containing Oxalic Acid. *Engineering* **2013**, *05* (09), 714–719. https://doi.org/10.4236/eng.2013.59085.

Supplementary Information

The role of Al^{3+}-based aqueous electrolytes in the charge storage mechanism of MnO_x cathodes

Véronique Balland, [†,*] *Mickaël Mateos,*[†] *Kenneth D. Harris,*[‡,§] *Benoît Limoges,*[†,*]

[†] Université de Paris, Laboratoire d'Electrochimie Moléculaire, UMR CNRS 7591, F-75013 Paris, France.

[‡] National Research Council Canada, Nanotechnology Research Centre, Edmonton, Alberta, T6G 2M9, Canada

[§] Department of Mechanical Engineering, University of Alberta, Edmonton, Alberta, T6G 2V4, Canada

I. Experimental Section

Chemicals. Acetic acid (Reagent plus, > 99%), KOH, HCl (Normapur, 37%), KCl (GR for analysis), ethanol absolute (EMSURE), $ZnCl_2$ (> 98%), $Zn(CF_3SO_3)_2$ (98%), $MnSO_4$ monohydrate (> 99%) were purchased from Sigma-Aldrich/Merck. $Al(CF_3SO_3)_3$ (99%) was purchased from Acros Organics. Anhydrous $AlCl_3$ (> 99%) was purchased from Fluka. $MnCl_2$ tetrahydrate (99%) was purchased from Alfa Aesar. Acetone (Normapur) and chloroform (Normapur) were purchased from VWR Chemicals.

GLAD-ITO Mesoporous Electrodes. Porous ITO thin films were prepared by the glancing angle deposition (GLAD) method followed by thermal treatment as previously described.[S1] Briefly, nanostructured ITO films were deposited from ITO evaporant (Cerac, 91:9 In_2O_3/SnO_2 99.99% pure) in an electron-beam physical vapor deposition system (Axxis, Kurt J Lesker) on ITO-coated glass substrates (8-12 Ω/□, Delta Technologies Ltd.). Throughout the deposition, substrates were maintained at an 80° angle with respect to impinging evaporant flux, while constantly rotating as a feedback-controlled function of the deposition rate. The film thickness was 1 µm. Following deposition, the GLAD-ITO samples were thermally annealed in a two stage process, first under air at 500 °C and subsequently under 5% H_2/Ar flow at 375 °C, to improve and stabilize the optical and electrical properties. For such deposition conditions, the film porosity was previously estimated to be 0.5 and its density to be 4 $g \cdot cm^{-3}$.[S1] Prior to the electrochemical experiments, the GLAD-ITO electrodes were cleaned by soaking them successively in chloroform, acetone, and ethanol, each time for 30 min at 50°C. After the electrodes were left to dry, a geometric area of 0.50 ± 0.1 cm^2 was delimited by depositing an insulating layer of nail polish. After cycling, GLAD-ITO electrodes were recycled by successively soaking 5 minutes in an aqueous acidic solution containing 3 %wt H_2O_2 and 30 minutes in a large volume of milliQ water.

Preparation of the MnO_2-coated GLAD-ITO electrodes. *Ex situ* electrodeposition of MnO_2 within the 3D structure of GLAD-ITO electrodes was performed by galvanostatic electrodeposition as previously described,[S2] using a standard three-electrode cell configuration and a multichannel potentiostat/galvanostat (VSP model, BioLogic instrument). Experiments were performed at room temperature, and an SCE (+0.244 V *vs.* NHE) and Pt-grid were used as reference and counter electrode, respectively. For electrodeposition, GLAD-ITO electrodes were

placed in 7 mL of a quiescent acetate buffer (1 M, pH 5.0) containing 0.1 mM $MnCl_2$ and 0.85 M KCl. After preconditioning by cyclic voltammetry (CV) from 0.35 to 0.75 V (3 cycles) at 100 $mV \cdot s^{-1}$, galvanostatic electrodeposition at 300 $\mu A \cdot cm^{-2}$ (normalized to the geometric electrode area) was performed to final deposited charges, Q_c, of 25 to 100 $mC \cdot cm^{-2}$ (see Fig. S1 for a typical set of electrochemical data). The as-prepared MnO_2-GLAD-ITO electrodes were next carefully rinsed with milliQ water and soaked 30 min in 1 M KCl aqueous solution to remove all traces of electrolyte prior to galvanostatic cycling. The modified electrodes' homogeneous brown color (see Fig. S2) is characteristic of uniform MnO_2 electrodeposition. We previously established that the quantity of electrodeposited MnO_2 (in $mg \cdot cm^{-2}$, normalized to the geometric electrode area) scales linearly with the deposited charge Q_c (in $C \cdot cm^{-2}$) according to the following relationship:[S2]

$$m_{MnO_2} = (0.484 \pm 0.008) \times Q_c$$

Preparation of the "MnO-based electrolyte". 7.1 mg/mL of MnO was added to a 2 m $Al(OTf)_3$ electrolyte and left for a few hours. The solution was then filtered to remove undissolved MnO. The filtrate of pH 1.6 was slightly yellow and it was then directly used with a fresh GLAD-ITO electrode for galvanostatic cycling.

Spectroelectrochemistry. Spectroelectrochemical experiments were performed in a quartz UV-visible cell modified to accommodate three electrodes with an electrolyte volume of 1.2 mL. The counter electrode was a Pt grid (0.06 mm wire diameter, 0.25 mm nominal space, Goodfellow) or a zinc foil (0.35 mm thickness, Goodfellow) and the reference electrode was a Dri-Ref Ag/AgCl/KCl_{sat} electrode (+0.2 V *vs*. NHE, WPI Instruments). Unless otherwise stated, all reported potentials are quoted against this reference electrode. The UV-visible absorption spectra were recorded in transmission mode using an HR-2000+ spectrometer (Ocean Optics) controlled by the SpectraSuite software. Spectra were obtained by averaging 50 individual spectra recorded with an integration time of 40 ms.

Zn/MnO_2 battery cell configuration. The cyclability of the Zn/MnO_2 cell assemblies (2-electrode configuration) was investigated in a glass cell containing a MnO_2-GLAD-ITO electrode as the cathode, a zinc foil (0.35 mm thickness, Goodfellow) as the anode (electroactive

surface area of 0.5 ± 0.1 cm^2 delimited by nail varnish), and 5 mL of aqueous electrolyte. The electrochemical cell was sealed with a septum to avoid evaporation of the aqueous electrolyte over long-term cycling (see Fig. S5).

Galvanostatic experiments. The (spectro)electrochemical cell was controlled by a VSP BioLogic potentiostat interfaced with EC-Lab 11.3 software. During the galvanostatic cycling experiments, a period of 30 s at the open circuit potential was systematically added at the end of each charge and discharge step to allow for relaxation of the potential. The charge was fixed to 100 $mC \cdot cm^{-2}$, with a duration cut-off of 200 s at 0.5 $mA \cdot cm^{-2}$. The charge and discharge cut-off potentials were fixed for the spectroelectrochemical experiments at +1.2 and +0.15 V *vs*. the Ag/AgCl reference electrode, and for cell assemblies at +2.5 and +0.5 V *vs*. the Zn counter electrode.

All gravimetric intensities ($A \cdot g^{-1}$) were calculated from the current density ($mA \cdot cm^{-2}$) applied to the electrode and the mass of MnO_2 electrodeposited *ex situ* (48.4 $\mu g \cdot cm^{-2}$). The Coulombic efficiency(CE), energetic efficiency (EE), and gravimetric capacity (C_g in $mA \cdot h \cdot g^{-1}$) were calculated using the following equations:

$$CE = \frac{Q_{i,disch}}{Q_{i,ch}} \quad ; \quad EE = \frac{E_{i,disch}}{E_{i,ch}} \quad ; \quad C_g = \frac{1000}{3.6}\frac{Q_{i,disch}}{0.484}$$

where $Q_{i,ch}$ and $Q_{i,disch}$ are the areal charging and discharging capacities of the i-th cycle in $mC \cdot cm^{-2}$, and $E_{i,ch}$ and $E_{i,disch}$ the corresponding charging and discharging energy densities in $W \cdot h \cdot cm^{-2}$ determined from the product of Q and the average charge/discharge voltages.

X-Ray fluorescence spectrometry (XRF). After cycling, the electrodes were soaked in milliQ water for a few minutes to remove the electrolyte and then left to dry at ambient temperature prior to analysis. A Panalytical Epsilon 3XL spectrometer, equipped with an Ag X-ray tube and operating under an He atmosphere, was used under 3 conditions, *i.e.* 50 kV–6 µA for 180 s to analyze In and Sn, 20kV–15 µA for 60 s to analyze Mn, and 5 kV–60 µA for 60 s to analyze Al. Calibrations were established by analyzing 1 g/L certified solutions of the 4 elements (Inorganic Ventures), and using exactly the same measurement conditions. For aluminium, the limit of

detection and limit of quantification were 47 and 156 ng, respectively, while for manganese, they were 17.5 ng and 58.5 ng, respectively.

In order to ensure equivalent surface area analysis for all samples, a delimited area of 0.16 cm^2 located within the electroactive surface area of the electrode was exposed to the X-Ray beam (through a steel mask). We noticed that a small amount of Mn was detected in bare GLAD-ITO electrodes, most likely arising from the commercial ITO-glass substrate. In all samples analyzed, the amount of Al detected was below the limit of quantification. For the electrodes loaded *ex situ*, a linear relationship was obtained between the *ex situ* charge Q_c of the electrode and the areal mass of Mn quantified by XRF (see Fig. S3). This confirms that XRF provides quantitative analysis of the Mn mass remaining over the surface of cycled GLAD-ITO electrodes. However, the m_{Mn} (in µg·cm^{-2}) deduced from XRF was systematically lower than that determined by ICP quantification, which is most likely due to uncertainties in both the exact surface exposed (notably because of the incidence angle of the X-Ray beam) as well as matrix effects. Therefore, the ICP data were used as a reference to adjust the XRF calibration plot in Fig. S3, leading to a correcting factor 1.347. The m_{MnO_2} (in µg·cm^{-2}) was finally calculated from m_{Mn} as determined by XRF according to the following equation:

$$m_{MnO_2} = \frac{87}{55} \times 1.347 \times \left(m_{Mn} - 1.91 \right)$$

II. Nernst Equation

The proton-coupled MnO_2-to-Mn^{2+} conversion reaction is characterized by the following Nernst equation:[3]

$$E = E^0_{MnO_2/Mn^{2+}} - 0.12 \times \mathrm{pH} - 0.03 \times \log\left(a_{Mn^{2+}} \right) \qquad \text{(S1)}$$

where $E^0_{MnO_2/Mn^{2+}}$ is the standard potential of the MnO_2/Mn^{2+} redox couple (*i.e.*, 1.15 V *vs.* Ag/AgCl),[S3] $a_{Mn^{2+}}$ is the activity of soluble Mn^{2+} ions, and the pH corresponds to the local value at the MnO_2/electrolyte interface. The latter is determined by the pK_a value of the acetic acid/acetate couple and by the relative local activities of acetic acid and acetate. These activities depend on the dynamic equilibrium between the fluxes of acetic acid/acetate molecules

consumed/generated *via* the MnO_2 electrodissolution and the fluxes of these same molecules arriving/leaving the electrode to compensate for the concentration gradients.[S3]

III. Supplementary Figures

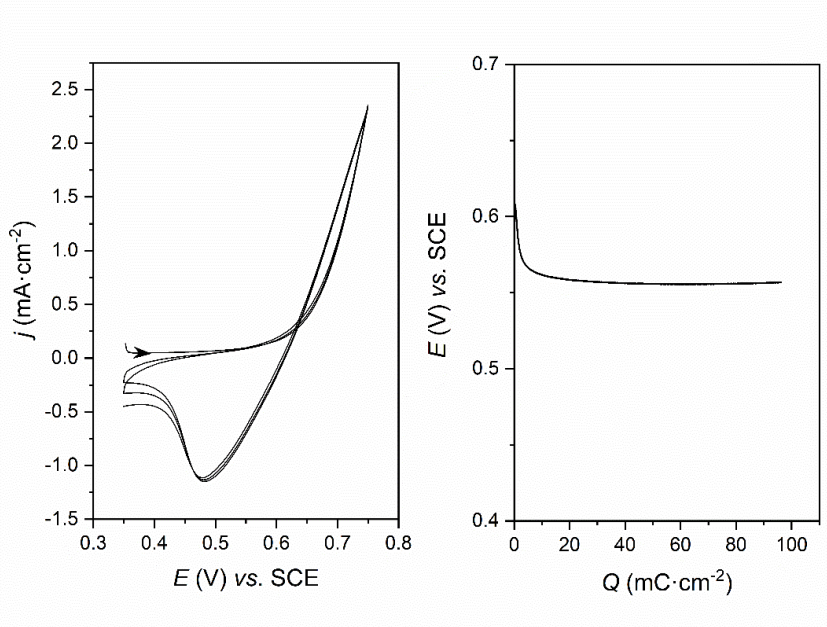

Figure S1. *Ex situ* electrochemical loading of the GLAD-ITO electrodes though successive (left) cyclic voltamogramms at 100 $mV \cdot s^{-1}$ followed (right) by a galvanostatic charge at 0.3 $mA \cdot cm^{-2}$.

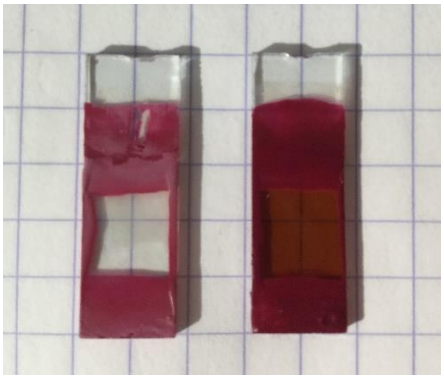

Figure S2. Photograph of the GLAD-ITO electrode (left) before and (right) after *ex situ* loading to 100 $mC \cdot cm^{-2}$.

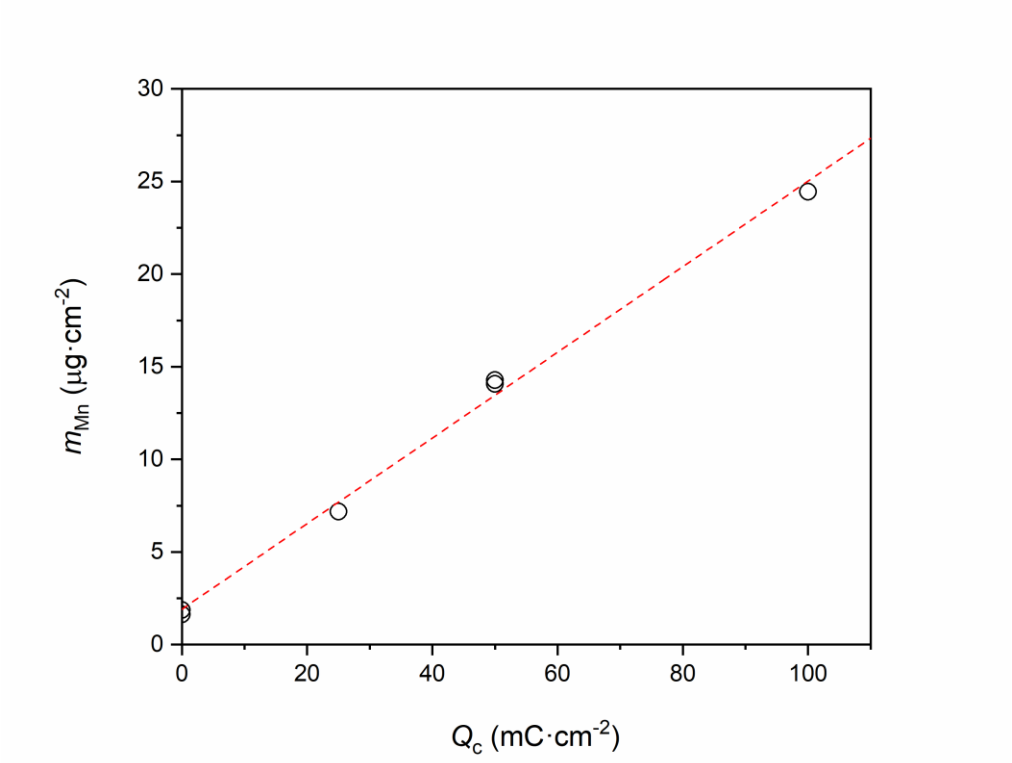

Figure S3. Linear relationship between the areal mass of Mn determined by XRF (normalized to the exposed geometric surface area) and the *ex situ* loading charge Q_c. The experimental data were fitted to a linear regression with a slope of 0.23, an intercept at 1.91, and a R^2 value of 0.995.

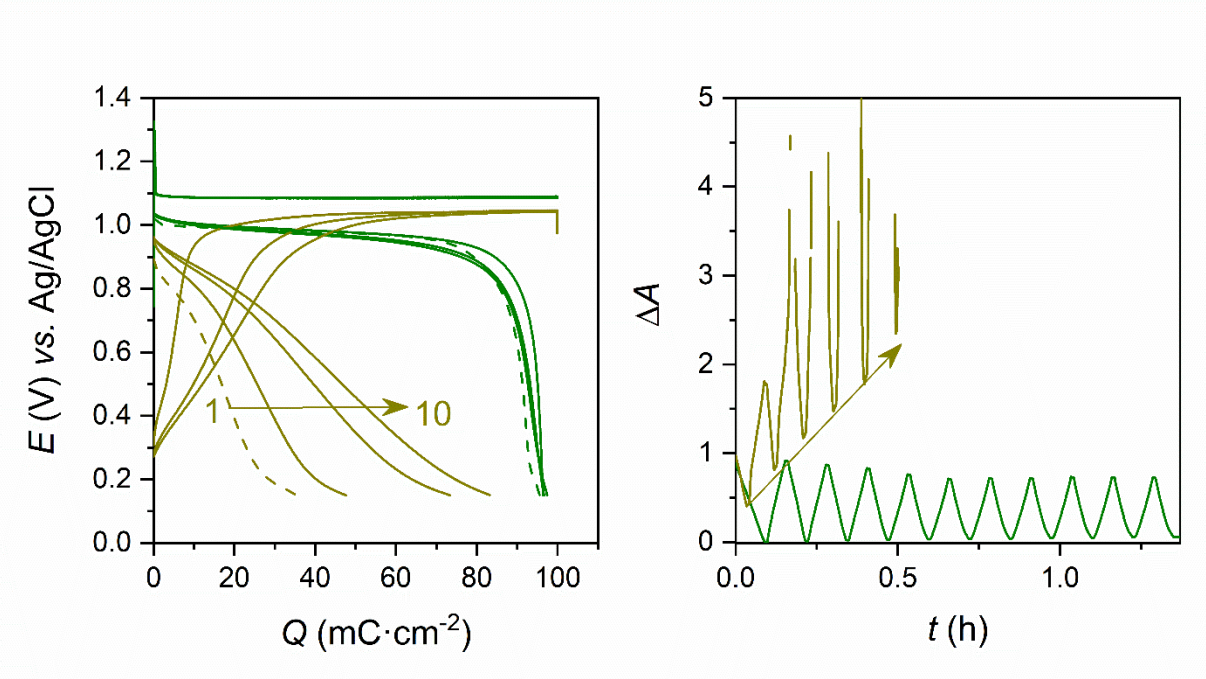

Figure S4. *In situ* spectroelectrochemical galvanostatic cycling of MnO_2-GLAD-ITO electrodes in a 2 M KCl aqueous electrolyte pre-equilibrated with 0.1 M $MnCl_2$ and adjusted with a 3 M HCl solution to (dark yellow) pH 2 and (green) pH 1. The first discharges (dashed lines) were performed at 0.3 $mA \cdot cm^{-2}$, while the subsequent 10 charge/discharge cycles (plain lines for 1st, 5th and 10th cycle) were performed at 0.5 $mA \cdot cm^{-2}$.

Comment. Upon discharging the MnO_2-GLAD-ITO electrode in a pH 2 electrolyte containing 2 M KCl and 0.1 M $MnCl_2$, a much lower capacity (as well as absorbance decrease) is recovered compared to that obtained in electrolytes containing either a 1 M acetic acid or an Al^{3+} salt (Table S1). At the end of the first discharge, the m_{MnO_2} value quantified from XRF indicates a residual amount as high as 60% of its initial value, confirming that only partial electrodissolution occurs during the discharge step. When the electrode is next subjected to a series of 10 charge/discharge cycles in the same electrolyte, we observe the back electrodeposition of MnO_2 as attested by the absorbance increase, which is also coupled to an acidification of the electrolyte. This allows for a progressive increase of the Coulombic efficiency during the subsequent cycles. *On contrario*, a higher quality initial discharge is observed in an electrolyte of similar chemical composition acidified to pH 1, translating into a higher capacity and higher *CE* value. This electrolyte allows us to reversibly electrodissolve/electrodeposit a fixed amount of MnO_2 as attested by the relatively stable absorbance oscillation.

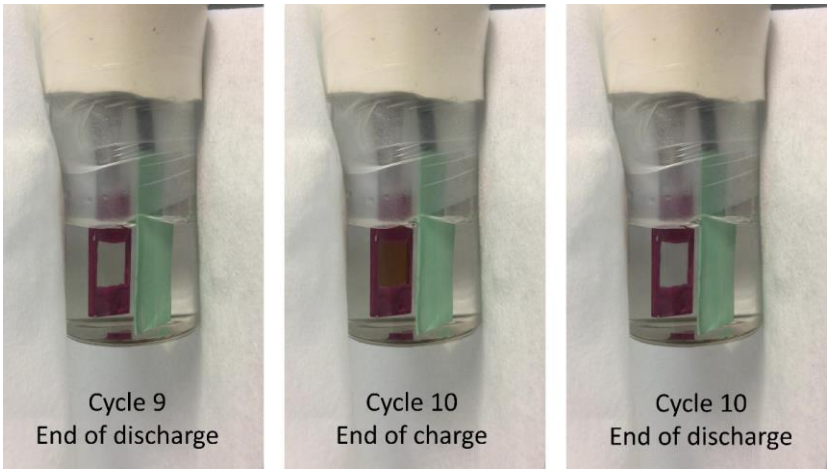

Figure S5. Photographs taken during the 10th galvanostatic cycle recorded at a Zn/MnO_2-GLAD-ITO assembly. Electrolyte: 1.25 M $Al(OTf)_3$, 0.1 M $ZnCl_2$, 0.1 M $MnCl_2$ (pH 1.5).

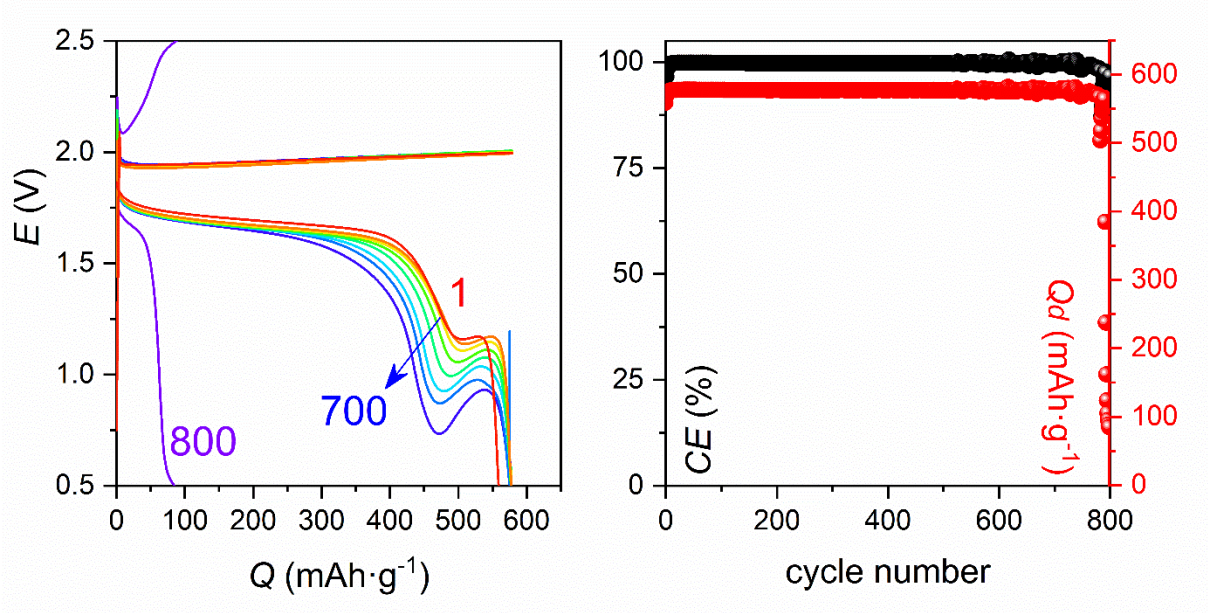

Figure S6. Long-term cycling of the Zn/MnO_2-GLAD-ITO assembly in 1 m $Al(OTf)_3$ + 1 m $Zn(OTf)_2$ + 0.1 m $MnSO_4$ (pH 1.75) solution at a rate of 10 $A \cdot g^{-1}$.

Comment. During long term cycling, the Zn/MnO_2-GLAD-ITO cell shows a progressive evolution of the shape of the discharge curve in contrast to the charge curve which overlaps perfectly. Then from the 780 cycle, a sudden loss of the cell charging capacity is noted over a few cycles, signalling the shutdown of the cell. For the moment, we have no explanation for this behaviour.

IV. Supplementary Tables

Table S1. Chemical composition of the aqueous electrolytes used for the spectroelectrochemical experiments and main features (potential, charge, absorbance and mass of Mn) of the *ex situ* galvanostatic charges and first *in situ* galvanostatic discharges.

	Electrolyte composition	**pH**	E_c (V *vs.* Ag/AgCl)	Q_c (mC·cm^{-2})	ΔA at end of the charge or of the 1st discharge	m_{MnO_2} (µg·cm^{-2}) at end of the charge or of the 1st discharge
Ex situ galvanostatic charge	1 M acetate buffer + 0.1 M $MnCl_2$ + 0.85 M KCl	5.0	0.600	100	0.86 ± 0.03	48
1st *in situ* galvanostatic discharge	1 M $AlCl_3$ + 0.1 M $MnCl_2$	2.10	0.767	97	0.01	-
	1 M $Al(OTf)_3$ + 0.1 M $MnCl_2$	1.98	0.750	96	0.02	0.3
	1 M acetic acid + 0.1 M $MnCl_2$ + 2 M KCl	2.05	0.742	92	0.04	1.9
	2 M KCl + 0.1 M $MnCl_2$ + acidified with 3 M HCl	2.05	0.415	43	0.33	28
	2 M KCl + 0.1 M $MnCl_2$ + acidified with 3M HCl	1.0	0.975	99	0.004	-

Table S2. **Concentration, molality and pH of aqueous electrolytes prepared from various Al^{3+}- or Zn^{2+}- inorganic in milliQ water.**

Salt	Al^{3+} or Zn^{2+} [a, b] Concentration (M in mol/L)	Al^{3+} or Zn^{2+} [a, b] molality (m in mol/kg)	pH
$Al(OTf)_3$	2	*3.7*	< 0
	1.4	2	1.4
	1	*1.3*	2.05
Anhydrous $AlCl_3$	2	*2.1*	0.85
	1		2.2
$Zn(OTf)_2$	2	*2.7*	3.8
	1.7	2	4.35
$Al(OTf)_3$ + $Zn(OTf)_2$	1 each		0.7
		1 each	1.75

[a] Solutions were prepared in a volumetric flask, to avoid volumetric issues associated to the high mass of salt required for concentrations in the molar range.

[b] Italic values were calculated from experimental data (*i.e.*, from mass of water added in the volumetric flask for electrolytes prepared in molarity or from final volume of the mixture for electrolytes prepared in molality)

Comment on the electrolyte preparation. Preparing aqueous electrolytes with inorganic salts at a molar concentration requires taking into account the volume occupied by the large amount of inorganic salt. This is especially true with triflate salts, which have very low density. We notice that this is not done in some publications mentioning molarities for electrolytes prepared from mixing a certain mass of the inorganic salt with a fixed volume of water without considering the volume expansion.[S4–S6] As an illustration, we prepared a "2 M $Al(OTf)_3$" aqueous electrolyte by mixing 10 mmol of Al(OTf) (4.74 g of the dry corresponding salt occupying a volume of ca. 4 mL) with 5 mL milliQ water. After complete dissolution of the inorganic salt, the final volume of the solution was 7.2 mL and its final mass was 9.72 g. Accordingly, the real concentration of the electrolyte is 1.4 $mol \cdot L^{-1}$ (instead of 2 M). We also measured the pH after the solution was left to recover ambient temperature (since dissolution is exothermic) and a value of 1.4 was determined.

Table S3. Main chemical and electrochemical features of the Zn/MnO_2-GLAD-ITO cell assemblies. *CE* and *EE* are average values over 100 cycles.

Electrolyte composition	pH	E_d (V)	ΔE [a] (V)	$CE \pm 3\sigma$ [b] (%)	$EE \pm 3\sigma$ [b] (%)
1 M $AlCl_3$, 0.25 M $ZnCl_2$, 0.1 M $MnCl_2$	1.9	1.76	0.24	99.3 ± 0.2	83.1 ± 1.8
1 M $Al(OTf)_3$, 0.1 M $ZnCl_2$, 0.1 M $MnCl_2$	1.77	1.65	0.25	98.6 ± 0.3	80.3 ± 1.5
1.25 M $Al(OTf)_3$, 0.1 M $ZnCl_2$, 0.1 M $MnCl_2$	1.5	1.70	0.29	99.6 ± 0.2	81.3 ± 2.8
1 m $Al(OTf)_3$, 1 m $Zn(OTf)_3$, 0.1 m $MnSO_4$	1.75	1.67	0.30	99.7 ± 1.2	80.0 ± 1.7

[a] Voltage hysteresis

[b] σ is the standard deviation

Comment on the bi-cation electrolyte. With the cycling of the Zn/MnO_2-GLAD-ITO assembly in an electrolyte containing 1 m $Al(OTf)_3$, 1 m $ZnCl_2$, and 0.1 m $MnSO_4$ at pH 1.4, we demonstrate that MnO_2-to-Mn^{2+} conversion is the main charge storage mechanism occurring at the cathode in such electrolyte. The corresponding charge/discharge potentials as well as potential hysteresis are very close to those reported for a Zn/α-MnO_2 assembly cycled in a (1 M $Al(OTf)_3$, 1 M $Zn(OTf)_2$, 0.1 M $MnSO_4$) bi-cation electrolyte (see Table 1).[S4] This result strongly supports a unified charge storage mechanism in both electrolytes. It is worth noting here that our attempts at dissolving 0.1 M $MnSO_4$ in a 1 M $Al(OTf)_3$ and 1 M $Zn(OTf)_2$ mixture were unsuccessful, which brings us to assume that the authors refer rather to molality than molarity (see comment below Table S2 on the electrolyte composition) and thus that the electrolyte compositions are in fact identical in both studies. Furthermore, we also demonstrate that similar electrochemical features are retrieved in an electrolyte made of a mixture of 1.25 M $Al(OTf)_3$, 0.1 M $ZnCl_2$, and 0.1 M $MnCl_2$ at a same pH (see Table 1). Thus, replacing most of the Zn^{2+} ions

with Al^{3+} ions does not affect the electrochemical features of the Zn/MnO_2 assembly, which is fully consistent with a cathode charge storage mechanism that does not rely on the reversible insertion of Zn^{2+} ions. Besides, the conversion mechanism allows us to rationalize the significant up-shift of the charge/discharge potentials (+ 0.26 V) reported by the authors upon switching from a 2 m $Zn(OTf)_2$ electrolyte to a mixture of 1 m $Al(OTf)_3$ and 1 m $Zn(OTf)_2$. Indeed, this is associated with a significant acidification of the electrolyte (we estimate a ΔpH value of -2.6 based on the data of Table S3). On account of the pH-independence of the Zn^{2+}-to-Zn electrochemical reaction and the pH-dependence of the MnO_2-to-Mn^{2+} conversion reaction within the pH range investigated, the +0.26 V up-shift translates into a pH decrease of 2.2, which is close to the ΔpH value between the mono-cation and the bi-cation electrolytes.

V. References

(S1) Krause, K. M.; Taschuk, M. T.; Harris, K. D.; Rider, D. A.; Wakefield, N. G.; Sit, J. C.; Buriak, J. M.; Thommes, M.; Brett, M. J. Surface Area Characterization of Obliquely Deposited Metal Oxide Nanostructured Thin Films. *Langmuir* **2010**, *26* (6), 4368–4376. https://doi.org/10.1021/la903444e.

(S2) Mateos, M.; Harris, K. D.; Limoges, B.; Balland, V. Nanostructured Electrode Enabling Fast and Fully Reversible MnO_2-to-Mn^{2+} Conversion in Mild Buffered Aqueous Electrolytes. *ACS* **2020**, *3*, 7610–7618. https://doi.org/10.1021/acsaem.0c01039.

(S3) Mateos, M.; Makivic, N.; Kim, Y.-S.; Limoges, B.; Balland, V. Accessing the Two-Electron Charge Storage Capacity of MnO_2 in Mild Aqueous Electrolytes. *Adv. Energy Mater.* **2020**, 2000332. https://doi.org/10.1002/aenm.202000332.

(S4) Li, N.; Li, G.; Li, C.; Yang, H.; Qin, G.; Sun, X.; Li, F.; Cheng, H. Bi-Cation Electrolyte for a 1.7 V Aqueous Zn Ion Battery. *ACS Appl. Mater. Interfaces* **2020**, *12*, 13790–13796. https://doi.org/10.1021/acsami.9b20531.

S5) Yan, C.; Lv, C.; Wang, L.; Cui, W.; Zhang, L.; Dinh, K. N.; Tan, H.; Wu, C.; Wu, T.; Ren, Y.; Chen, J.; Liu, Z.; Srinivasan, M.; Rui, X. Architecting a Stable High-Energy Aqueous Al-Ion Battery. *J. Am. Chem. Soc.* **2020**, *142*, 15295615304. https://doi.org/10.1021/jacs.0c05054.

(S6) He, S.; Wang, J.; Zhang, X.; Chen, J.; Wang, Z.; Yang, T.; Liu, Z.; Liang, Y.; Wang, B.; Liu, S.; Zhang, L.; Huang, J.; Huang, J.; Dell, L. A. O.; Yu, H. A High-Energy Aqueous Aluminum-Manganese Battery. *Adv. Funct. Mater.* **2019**, 1905228. https://doi.org/10.1002/adfm.201905228.